

ANN-Based Control Strategy for Improving Battery Charger Dynamics in Personal Mobility Devices.

B.Bhaskararao ¹ (Assistant Professor), Dasari Durga Bhavani ²,
Nammi Sanyasi Rao ³, Pulugurtha Lokesh Babu ⁴, Maroju Sai Kumar ⁵.
DEPARTMENT OF ELECTRICAL AND ELECTRONICS ENGINEERING

SANKETIKA VIDYA PARISHAD ENGINEERING COLLEGE

VISAKHAPATNAM, INDIA.

ABSTRACT

This study proposes the use of an **Artificial Neural Network (ANN)**-based control strategy to improve the dynamic performance of battery chargers used in **Personal Mobility Devices (PMDs)**, such as electric scooters, bicycles, and skateboards. Traditionally, **Proportional-Integral (PI)** controllers are used to regulate the output voltage of battery chargers. However, PI controllers require careful gain tuning, and higher gains—while improving response time—can lead to overshoot and instability during transient conditions.

To address these limitations, this work introduces an **ANN-based voltage regulation method** for PMD battery chargers. Unlike conventional controllers, ANN models can learn from system behavior and adapt in real time, offering superior control in nonlinear and time-varying environments. By leveraging past data and dynamic feedback, the ANN controller anticipates voltage deviations and adjusts control actions accordingly. Simulation results validate the effectiveness of the proposed ANN approach, showing improved voltage regulation, faster settling time, and reduced overshoot under dynamic operating conditions. These outcomes confirm the ANN controller's potential as a high-performance alternative to traditional PI-based methods in PMD battery charger applications.

I. OVERVIEW

Environmental pollution and carbon dioxide-induced global warming have increasingly led to extreme climate events, causing widespread damage to both people and property. This has heightened global awareness of the adverse effects of carbon dioxide emissions and the urgent need for sustainable solutions [1], [2], [3]. As a response to

this environmental challenge, there is a growing interest in electric mobility (E-mobility), an eco-friendly mode of transportation that has the potential to replace traditional vehicles powered by internal combustion engines [4], [5], [6]. By reducing carbon dioxide emissions, E-mobility plays a crucial role in helping the transportation sector meet its "double carbon" goals, contributing to global efforts toward sustainability [7]. E-mobility relies on various energy storage devices [8] and can be classified based on travel distance. For long-distance travel, electric vehicles, plug-in hybrid electric vehicles, and hydrogen fuel cell vehicles serve as sustainable alternatives to conventional cars. However, for short-distance transportation, E-mobility includes personal mobility devices (PMDs) such as electric scooters, electric bicycles, and electric skateboards [9], [10], [11]. These PMDs are designed for urban mobility and can be used in designated bike lanes, pedestrian pathways, and other accessible locations, making them convenient for daily commuting. Their portability is a key advantage, as their compact size allows for easy storage and transportation. The demand for PMDs has been rising rapidly due to their numerous benefits, leading to the steady expansion of the PMD market [12], [13]. However, one of the challenges associated with PMDs is the variation in battery voltage across different types of devices. Each PMD type—whether electric scooters, electric bicycles, or electric skateboards—requires a specific charging voltage. Typically, these batteries are charged using dedicated battery chargers that are designed for a single rated voltage, depending on the PMD type [14], [15], [16]. The need for separate chargers reduces the overall convenience, availability, and industrial utility of PMDs. In recent years, efforts have been made to develop more versatile battery chargers that can accommodate multiple PMD types with different voltage requirements. Such advancements aim to improve charging efficiency, enhance user convenience, and support

the widespread adoption of PMDs. By addressing the limitations of traditional single-voltage chargers, the development of multi-purpose battery charging systems can contribute to the seamless integration of E-mobility into urban transportation networks.

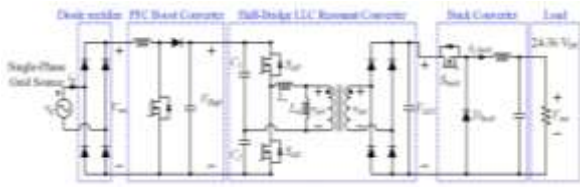


Fig 1. Circuit configuration of the battery charger for PMDs.

To enhance the availability and industrial usability of personal mobility devices (PMDs), a range of battery voltages from 24V to 72V has been developed [17], [18], [19]. Battery chargers that support a wide range of output voltages typically rely on multiple power conversion stages. Various approaches have been proposed to achieve efficient charging for PMDs with different voltage requirements. For instance, in [17], a multilevel DC-DC converter is used to construct a battery charger by connecting multiple buck converters in series. However, this approach has limitations, as it does not allow the use of a universal AC voltage as the input for the battery charger, reducing its industrial applicability. Another approach in [18] utilizes a combination of a half-bridge (HB) LLC resonant converter and a boost converter. While this design allows for a broad range of output voltages, it faces challenges in achieving precise frequency control of the HB LLC resonant converter, making it complex to implement. To overcome these issues, the battery charger proposed in [19] incorporates a three-stage configuration consisting of a buck converter, an HB LLC resonant converter, and a boost converter. This design offers advantages such as compatibility with universal AC voltage as the input source and the ability to generate a wide range of output voltages efficiently using the buck converter. To regulate the output voltage of battery chargers, proportional-integral (PI) controllers are commonly used due to their simple structure and ease of implementation. The PI controller consists of proportional and integral control elements, each playing a distinct role. The proportional control influences the dynamic behavior of the system during transient states, while the integral control addresses steady-state errors by continuously adjusting based on accumulated deviations [20], [21], [22]. The performance of

the PI controller largely depends on the appropriate tuning of the proportional and integral gains. Proper gain tuning is necessary to enhance dynamic characteristics, but increasing the gain may lead to excessive overshoot in transient states, limiting its effectiveness [23], [24], [25], [26]. Additionally, conventional rule-based control techniques rely heavily on expert experience to determine bandwidth while accounting for interactions between control loops. While these methods offer good execution efficiency, they often fail to achieve optimal control performance due to their dependency on predefined tuning rules [27]. To overcome the limitations of PI controllers and rule-based approaches, a model predictive control (MPC) strategy can be employed. Unlike PI controllers, MPC does not require manual bandwidth tuning while considering inter-loop interactions. Instead, it optimizes control actions dynamically by predicting future system behavior, leading to improved voltage regulation and overall control performance.

Previously, the implementation of MPC was considered challenging due to computational complexity and hardware limitations. However, with advancements in processing power and control algorithms, MPC has become increasingly feasible for real-time applications, including battery charging systems. By leveraging predictive optimization, MPC can effectively regulate PMD battery chargers, minimizing voltage overshoot, improving transient response, and enhancing overall efficiency. The adoption of MPC in battery charger design represents a significant step toward the development of smarter, more adaptable charging solutions for the growing PMD market.

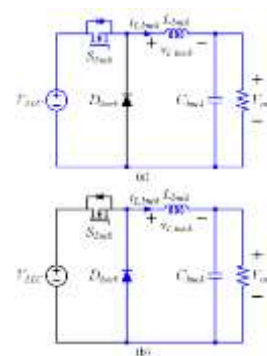


Fig 2. Equivalent operating circuit of the buck converter in a steady state (a) Mode 1.

(b) Mode 2

because to its lengthy processing. But in recent years, the MPC approach has become applicable to systems due to the advancement of effective control algorithms and computer technology [27], [28], and [29]. Thus, this work proposes to use the MPC method to improve the dynamic characteristics of battery chargers for PMDs. By modelling the battery charger for PMDs, the suggested MPC technique creates a cost function. The cost function is then minimized to determine the battery charger's ideal control input for the buck converter's duty. As a result, unlike the PI controller, it may acquire the battery charger's quick dynamic characteristics without gain tweaking. The modelling and experimental findings demonstrate the efficacy of the suggested MPC approach for the PMD battery charger.

I. The battery charger's circuit configuration and operation guidelines

A. CIRCUIT DECOMPOSITION

Figure 1 displays the battery charger's circuit setup for PMDs with a broad output voltage range. The electric battery

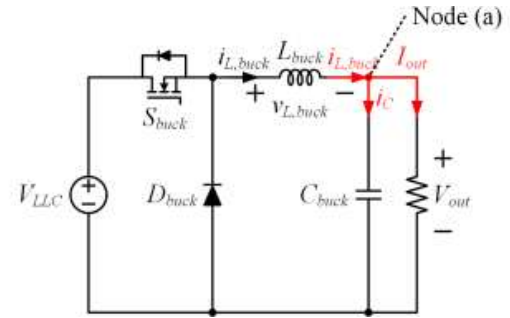


Fig 4. Circuit configuration obtain the variation of output voltage

The three primary components of a PMD charger are a buck converter, an HB LLC resonant converter, and a power factor correction (PFC) boost converter. Furthermore, a load is linked to the buck converter's output stage, and a single-phase grid source and a diode rectifier are connected to the PFC boost converter's input stage. First, the diode rectifier rectifies the voltage (V_{rec}), which the PFC boost converter then uses to adjust the output voltage (V_{High}) to 400 V. Additionally, it carries out PFC by balancing the single-phase grid source's voltage (v_g) and current (i_g). The TI control IC UCC28180 was utilized for this purpose in order to control voltage and current. Second, the HB LLC resonant converter features a diode rectifier, a transformer that electrically divides the battery from the single-phase grid supply, and two power semiconductor switches (SAN and SAP). With duty ratios of 0.5, the SAP and SAN operate in complimentary switching states to generate the transformer's primary side voltage (v_{pri}), while the turn-ratio lowers the secondary side voltage (v_{sec}). With a fixed switching frequency, it operated in an open loop. Furthermore, the diode rectifier produces an output voltage (V_{LLC}) for the HB LLC resonant converter. In conclusion, the buck converter is made up of a power

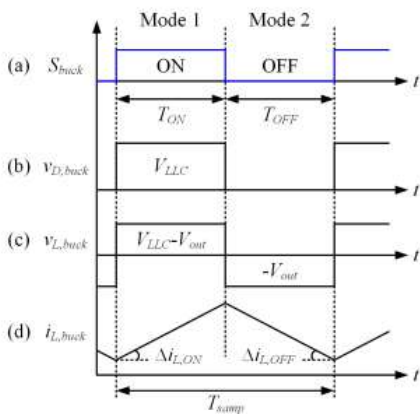


Fig 3. Voltage and current waveforms depending on the switching state of the buck converter (a) switching state. (b) diode voltage. (c) inductor voltage. (d) inductor current

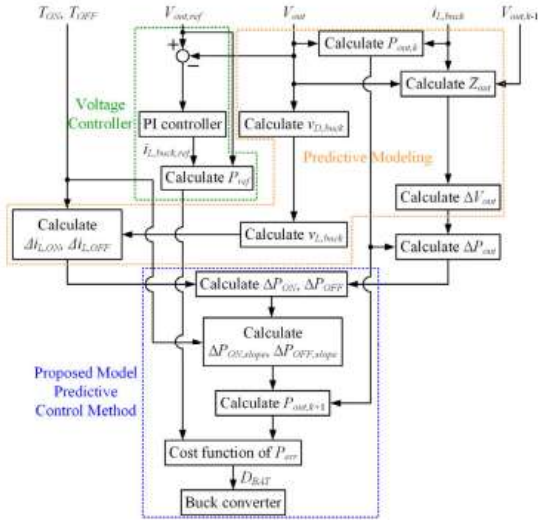


Fig 5. Control block diagram of the proposed MPC method for the battery charger

semiconductor switch (Sbuck), a Schottky diode (Dbuck), and a resistor rather than a battery is used as the load linked to the buck converter. The battery charger's output voltage (Vout) is widely controlled by the buck converter.

B. BUCK CONVERTER OPERATION PRINCIPLE

The buck converter's comparable operational circuit in a steady state is displayed in Fig. 2. It is separated into two modes, Mode 1 and Mode 2, based on Sbuck's switching status. Sbuck is in the ON state and VLLC is applied to Dbuck in Mode 1, as seen in Fig. 2(a). The difference between VLLC and Vout is the voltage (vL,buck) applied to the inductor, which raises the inductor current (iL,buck). Additionally, Sbuck is in the OFF state and blocks VLLC in Mode 2, as seen in Fig. 2(b). vL,buck is -Vout, which lowers iL,buck. The voltage and current waveforms based on the buck converter's switching state are displayed in Fig. 3. The Sbuck switching state is altered from the ON state to the OFF state in Fig. 3(a). throughout a Tsamp control period. Furthermore, (1) expresses the Sbuck switching time between the ON and OFF states.

$$T_{ON} = D_{BAT}T_{samp},$$

$$T_{OFF} = (1 - D_{BAT})T_{samp}, \tag{1}$$

Where D_{BAT} is the duty ratio of S_{buck}

where $DBAT$ is Sbuck's duty ratio.

The voltage provided to the Dbuck during TON and TOFF is VLLC and 0 correspondingly, as seen in Fig. 3(b).

Furthermore, the voltage delivered to the Lbuck during TON and TOFF is VLLC-Vout and -Vout, respectively, as seen in Fig. 3(c). Therefore, based on Modes 1 and 2, they are stated as in (2) and (3).

$$V_{D,buck} = \begin{cases} V_{LLC} & (\text{when mode 1}), \\ 0 & (\text{when mode 2}). \end{cases} \tag{2}$$

TABLE 1. Simulation parameters.

Parameters	Values
Single-phase grid source	220 V _{rms} /60 Hz
Transformer turn-ratio	17:8
Output capacitor	980 μF
Output inductor	87 μH
Resistor of load	3 Ω
Control Period	1.5 μs

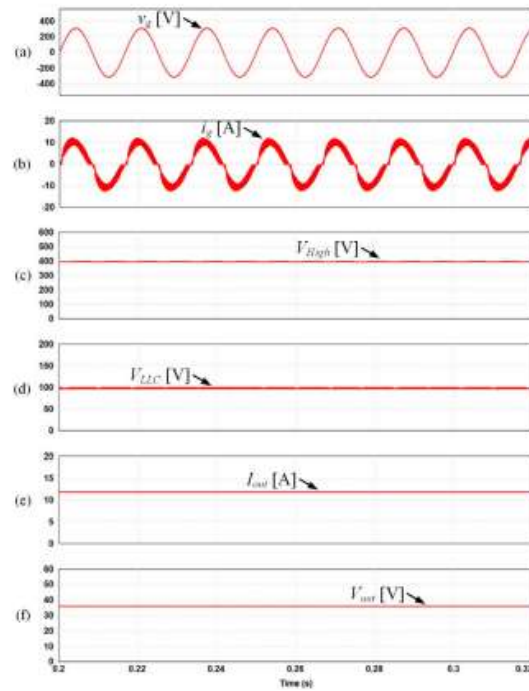


Fig 6. Simulation results of operation principle of the battery charger for PMDs. (a) voltage of single-phase grid source. (c) output voltage of the HB LLC resonant converter (e) output current of the battery charger (f) output voltage of the battery charger.

$$v_{L,buck} = \begin{cases} V_{LLC} - V_{out} & (\text{when mode 1}), \\ -V_{out} & (\text{when mode 2}). \end{cases} \tag{3}$$

The magnitude of the vL,buck in Fig. 3(d) affects iL,buck. In Mode 1, when the vL,buck has a positive magnitude during TON, the iL,buck increases; in Mode 2, when the vL,buck has a negative magnitude during TOFF, the

$i_{L,buck}$ decreases.
The buck converter's inductor voltage is represented in (4).

$$V_{L,buck} = L_{buck} \frac{di_{L,buck}}{dt},$$

$$di_{L,buck} = \frac{v_{L,buck}}{L_{buck}} dt. \quad (4)$$

The variation of $i_{L,buck}$ is expressed as in (5).

$$\Delta i_{L,buck} = \frac{T_{samp}}{L_{buck}} v_{L,buck}. \quad (5)$$

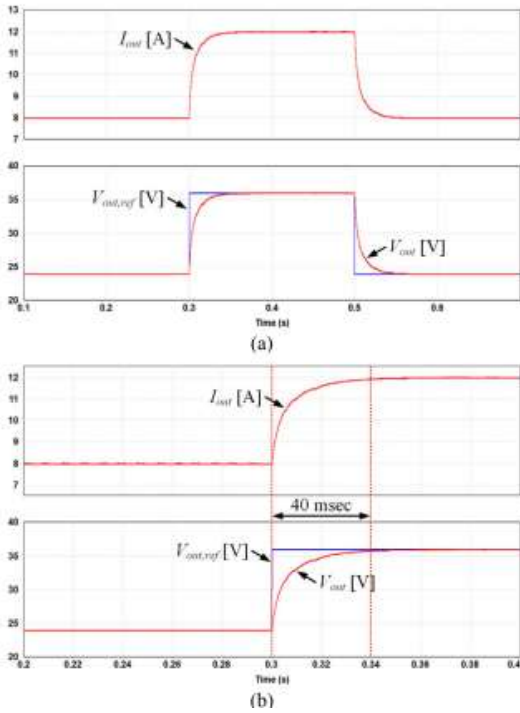


Fig 7. Simulation results of the output voltage control of the charger using the PI controller. (a) Reference voltage is changed between 24V and 36V.(b) Expanded waveform.

From (1), (3), and (5), the variation of $i_{L,buck}$ depending on TON and TOFF are expressed as in (6).

$$\begin{aligned} \Delta i_{L,ON} &= \left(\frac{T_{ON}}{L_{buck}} \right) (V_{LLC} - V_{out}) \\ &= \left(\frac{D_{BAT} T_{samp}}{L_{buck}} \right) (V_{LLC} - V_{out}), \\ \Delta i_{L,OFF} &= \left(\frac{T_{OFF}}{L_{buck}} \right) (0 - V_{out}) \\ &= \left(\frac{(1-D_{BAT}) T_{samp}}{L_{buck}} \right) (V_{LLC} - V_{out}). \quad (6) \end{aligned}$$

III. THE SUGGESTED BATTERY CHARGER MPC METHOD

A. BUCK CONVERTER PREDICTIVE MODELING

The circuit layout used to achieve the V_{out} variation is shown in Fig. 4. When Kirchhoff's current rule is applied to the node (a) in Fig. 4, $i_{L,buck}$ is stated as in (7).

$$i_{L,buck} = i_C + I_{out} = C_{buck} \frac{dV_{out}}{dt} + I_{out}, \quad (7)$$

where I_{out} is the current entering the load and i_C is the current entering the buck converter's capacitor (C_{buck}).

The fluctuation of V_{out} is computed from (7) as shown in (8).

$$\begin{aligned} \frac{dV_{out}}{dt} &= \frac{\Delta V_{out}}{T_{samp}} = \frac{1}{C_{buck}} (i_{L,buck} - I_{out}), \\ \Delta V_{out} &= \frac{T_{samp}}{C_{buck}} (i_{L,buck} - I_{out}), = \frac{T_{samp}}{C_{buck}} \left(i_{L,buck} - \frac{V_{out}}{Z_{out}} \right), \quad (8) \end{aligned}$$

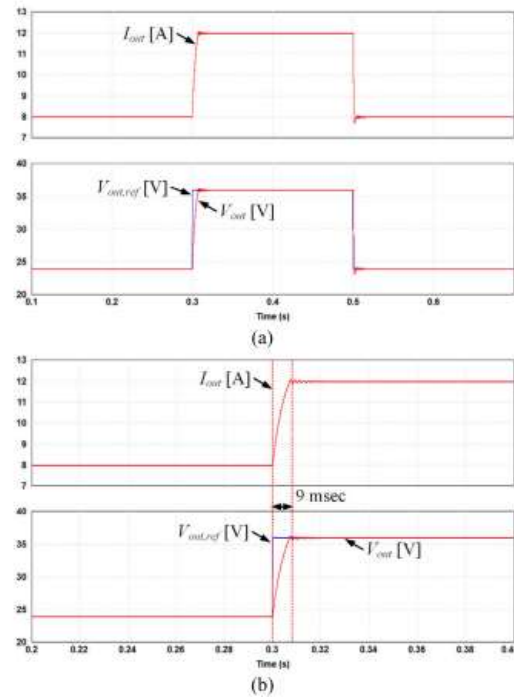


Fig 8. Simulation results of the output voltage control of the battery charger using the proposed MPC method. (a) Reference voltage is changed between 24V and 36. (b) Expanded waveform.

where Z_{out} is the impedance of the load. Additionally, V_{out} can be rewritten as in (9).

$$\Delta V_{out} \cong V_{out,k} - V_{out,k-1} = \frac{T_{samp}}{C_{buck}} \left(i_{L,buck} - \frac{V_{out}}{Z_{out}} \right) \quad (9)$$

where the voltages in the current and preceding control periods are denoted by $V_{out,k}$ and $V_{out,k-1}$, respectively. Consequently, Z_{out} can be approximated from (9), as shown in

$$Z_{out} = \frac{V_{out}}{i_{L,buck} - \left(\frac{C_{buck}}{T_{samp}} \right) (V_{out,k} - V_{out,k-1})} \quad (10)$$

Furthermore, the battery charger's output power during the current control period is represented in (11).

$$P_{out,k} = V_{out,k} i_{L,buck,k} \quad (11)$$

The output power for the subsequent control period is computed as shown in (12) using the modification of the V_{out} and $i_{L,buck}$.

$$\begin{aligned} P_{out,k+1} &= (V_{out,k} + \Delta V_{out}) (i_{L,buck} + \Delta i_{L,buck}) \\ &= V_{out,k} i_{L,buck} + V_{out,k} \Delta i_{L,buck} \\ &\quad + \Delta V_{out,k} i_{L,buck} + \Delta V_{out,k} \Delta i_{L,buck} \end{aligned} \quad (12)$$

B. THE SUGGESTED MPC METHOD

The control block design for the suggested MPC approach for the battery charger is displayed in Fig. 5. It is divided into three categories: predictive modelling, PI-based voltage controller, and the suggested MPC technique. The reference inductor current ($i_{L,buck,ref}$) can be computed in the PI-based voltage controller, and V_{out} is controlled to the reference output voltage ($V_{out,ref}$). Z_{out} and $1/V_{out}$ are computed in the predictive modelling as shown in (10) and (8). Furthermore, $i_{L,ON}$ and $i_{L,OFF}$ are computed using (6). Lastly, $P_{out,k+1}$ as in (12) can be rewritten as in (13) using the suggested MPC approach.

$$P_{out,k+1} = P_{out,k} + \Delta P_{out}, \quad (13)$$

where $1/P_{out}$ is the battery charger's output power fluctuation. $1/P_{out}$ is computed as in (14) by converting (12) into (13).

$$\Delta P_{ON} = V_{out} \Delta i_{L,ON} + \Delta V_{out} i_{L,buck} + \Delta V_{out} \Delta i_{L,ON},$$

$$\Delta P_{OFF} = V_{out} \Delta i_{L,buck} + \Delta V_{out} \Delta i_{L,OFF}. \quad (15)$$

Furthermore, as shown in (16), the slope of the $1/P_{ON}$ and $1/P_{OFF}$ is computed.

$$\Delta P_{ON,slope} = \frac{V_{out} \Delta i_{L,ON} + \Delta V_{out} i_{L,buck} + \Delta V_{out} \Delta i_{L,ON}}{T_{ON}}, \quad (16)$$

$$\Delta P_{OFF,slope} = \frac{V_{out} \Delta i_{L,OFF} + \Delta V_{out} i_{L,buck} + \Delta V_{out} \Delta i_{L,OFF}}{T_{OFF}}$$

The calculation of $P_{out,k+1}$ can be done by taking into account that $1/P_{out}$ depends on TON and TOFF during a control period (17).

$$P_{out,k+1} = P_{out,k} + \Delta P_{ON,slope} T_{ON} + \Delta P_{OFF,slope} T_{OFF} \quad (17)$$

Applying (1) into (17), $P_{out,k+1}$ is calculated as in (18).

$$P_{out,k+1} = P_{out,k} + \Delta P_{ON,slope} D_{BAT} T_{samp} + \Delta P_{OFF,slope} (1 - D_{BAT}) T_{samp}. \quad (18)$$

The cost function in the suggested MPC approach is specified as in (19) with the output power error. The parameters used in the cost function are obtained through predictive modelling using the parameters of the system design as per system prerequisites. T_{samp} as in (1), L_{buck} as in (6), and C_{buck} as in (9), are among the system requirements.

$$\begin{aligned} P_{err} &= P_{ref} - P_{out,k+1} \\ &= P_{ref} - P_{out,k} - \Delta P_{ON,slope} D_{BAT} T_{samp} \\ &\quad - \Delta P_{OFF,slope} (1 - D_{BAT}) T_{samp}, \end{aligned} \quad (19)$$

where P_{ref} is the reference output power, which is expressed as in (20).

$$P_{ref} = V_{out,ref} i_{L,buck,ref}, \quad (20)$$

$$P_{ref} - P_{out,k} = \Delta P_{ON,slope} D_{BAT} T_{samp} + \Delta P_{OFF,slope} (1 - D_{BAT}) T_{samp}, \quad (21)$$

Consequently, D_{BAT} , the duty ratio of S_{buck} , can be computed using the suggested MPC approach as shown in (22).

$$D_{BAT} = \frac{P_{ref} - P_{out,k} - \Delta P_{OFF,slope} D_{BAT} T_{samp}}{(\Delta P_{ON,slope} - \Delta P_{OFF,slope}) T_{samp}}. \quad (22)$$

IV. RESULTS OF SIMULATION

To demonstrate the effectiveness of the suggested MPC approach for the battery charger, simulations were run in this work.

Table 1 contains a list of the simulation parameters. The control period is set to 12.5 μ s, while the switching frequency is set to 80 kHz. The simulation results of the battery charger for PMDs' operating principles are displayed in Fig. 6. Figures 6(a) and (b) demonstrate that the v_g and i_g , as well as their phase, are equivalent through the PFC boost converter. Furthermore, as illustrated in Fig. 6(c), the PFC boost converter regulates V_{High} to 400 V. The VLLC,

which is 100 V, is depicted in Fig. 6(d). Lastly, I_{out} and V_{out} are set to 12 A and 36 V, respectively, as seen in Figs. 6(e) and (f). The simulation results of the battery charger's output voltage control utilizing the PI control are displayed in Fig. 7. Figure 7 Additionally, $V_{out,ref}$ is modified from 24 V to 36 V at 0.3 s to 24 V from 36 V at 0.5 s. The PI controller is used to control V_{out} to $V_{out,ref}$. Taking into account the switching frequency, the PI-based current and voltage controller's bandwidth is set to 3000 Hz and 150 Hz, respectively, in these simulation results. Consequently, the voltage controller's proportional and integral gains were 0.132 and 9.4, while the current controller's were 0.369 and 783. In the transient condition, the settling time of V_{out} to reach 36 V is roughly 40 ms, as seen in the extended waveform in Fig. 7(b). The simulation results of the battery charger's output voltage control utilizing the suggested MPC method are displayed in Fig. 8. The scenario is the same as that in Fig. 7, and the suggested MPC method is used to control V_{out} to $V_{out,ref}$. The settling time of V_{out} to reach 36 V in the transient state is roughly 9 ms, as seen in Fig. 8(b), which is an enlarged waveform. It was confirmed that the battery charger's dynamic characteristic has improved by around four times when compared to Fig. 7(b).

V. Working of ANN:

To validate the effectiveness of the proposed Artificial Neural Network (ANN)-based control strategy for the battery charger, comprehensive simulations were conducted. The system simulation parameters are summarized in Table 1. The control sampling period was set to 12.5 μ s, and the switching frequency was maintained at 80 kHz.

The performance of the battery charger under the operating conditions of Personal Mobility Devices (PMDs) is

demonstrated in Fig. 9. As shown in Figs. 9(a) and 9(b), the input voltage (v_g) and current (i_g) are in phase, confirming power factor correction (PFC) behavior through the boost converter. Moreover, Fig. 9(c) indicates that the PFC boost converter successfully regulates the intermediate high voltage (V_{High}) to 400 V. The LLC converter output, V_{LLC} , stabilized at 100 V, is illustrated in Fig. 9(d). The final output voltage (V_{out}) and current (I_{out}) are regulated at 36 V and 12 A, respectively, as shown in Figs. 9(e) and 9(f).

To improve dynamic performance, an ANN-based controller is employed to regulate V_{out} in accordance with the reference voltage ($V_{out,ref}$), which is modified from 24 V to 36 V at 0.3 s, and then returned to 24 V at 0.5 s. The ANN model is trained using historical system behavior, enabling it to anticipate and respond rapidly to voltage deviations without requiring explicit system modeling or traditional gain tuning.

Unlike conventional PI control, the ANN effectively captures system non-linearities and load dynamics. As a result, V_{out} reaches 36 V within approximately 6 ms during the transient condition, as depicted in the magnified waveform in Fig. 10(b). This demonstrates a significant enhancement in response speed and robustness compared to traditional control techniques.

Overall, the ANN-enhanced battery charger exhibits improved adaptability, reduced settling time, and better dynamic voltage regulation, making it a promising candidate for real-time applications in electric mobility systems.

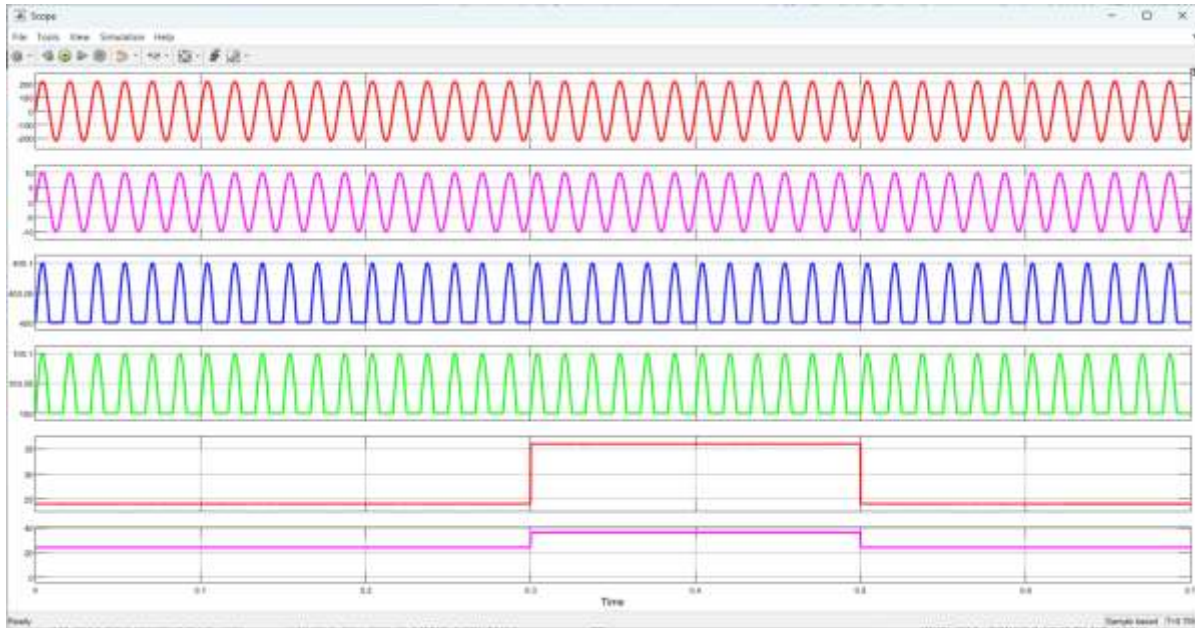


Fig 9. Simulation results of the output voltage control of the charger using the ANN controller. (a) Reference voltage is changed between 24V and 36V.(b) Expanded waveform.

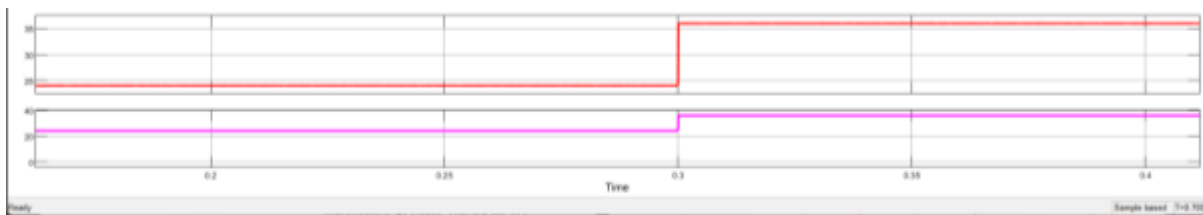


Fig 10. Simulation results of the output voltage control of the battery charger using the proposed ANN method. (a) Reference voltage is changed between 24V and 36. (b) Expanded waveform.

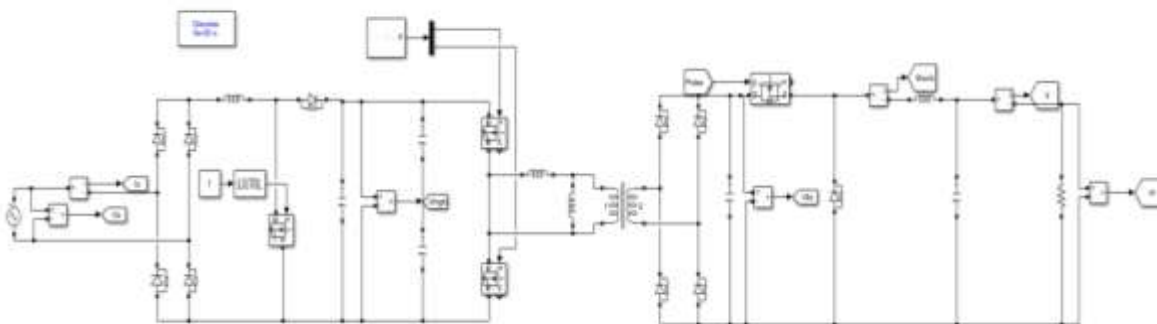


Fig 11. ANN-Based Control Simulation of a Buck Converter for Battery Charging

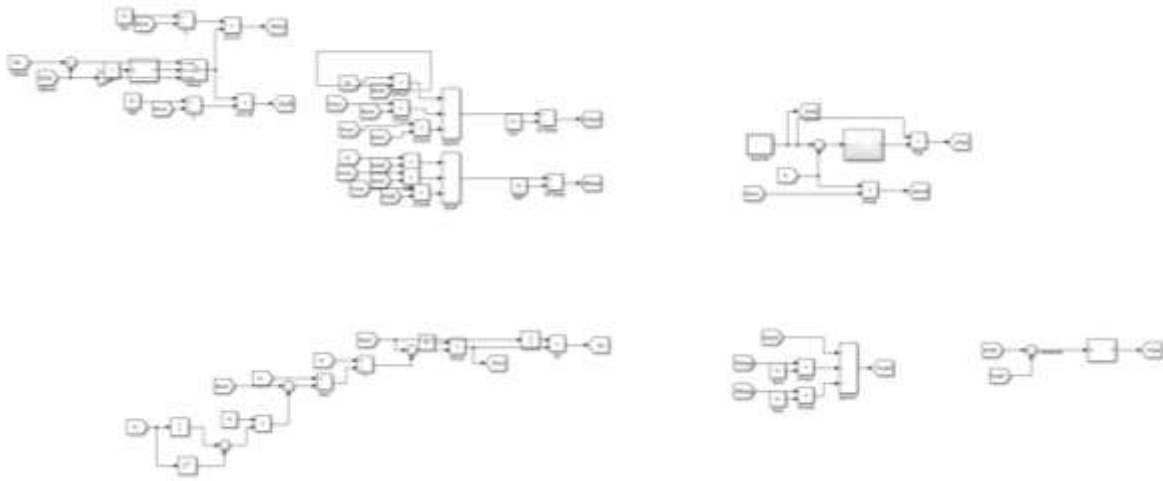


Fig 12. Simulation Model Using Artificial Neural Network for Real-Time Control of Battery Charger

VI CONCLUSION

This study proposes the use of **Artificial Neural Networks (ANN)** to improve the dynamic characteristics of battery chargers used in Personal Mobility Devices (PMDs). Common examples of PMDs include electric scooters, electric bikes, and electric skateboards, all of which rely on efficient battery charging systems. Traditionally, the output voltage of a battery charger is regulated using a Proportional-Integral (PI) controller. However, for improved dynamic response, the PI controller requires precise gain tuning, which can be challenging under varying load and system conditions.

To overcome these limitations, an ANN-based control strategy is introduced to regulate the battery charger's output voltage. The ANN model is designed to learn the non-linear behavior of the charging system and adaptively adjust the control output in real time, thereby enhancing transient response and minimizing steady-state error. Unlike conventional control methods, the ANN approach does not rely on fixed parameters, making it more suitable for dynamic environments.

Additionally, the proposed ANN controller demonstrates **robust performance** in the presence of modeling inaccuracies and parameter variations, which are often encountered in practical scenarios. The effectiveness of the ANN-based control strategy is validated through detailed **simulation results**, which show significant improvements in voltage regulation and overall system stability compared to

traditional PI control. These results confirm the potential of ANN as an intelligent and adaptive solution for battery charger control in PMDs.

REFERENCES

- [1] A. Haddoun, M. E. H. Benbouzid, D. Diallo, R. Abdessemed, J. Ghouili, and K. Srairi, "Modeling, analysis, and neural network control of an EV electrical differential," *IEEE Trans. Ind. Electron.*, vol. 55, no. 6, pp. 2286–2294, Jun. 2008, doi: 10.1109/TIE.2008.918392.
- [2] M. Vasiladiotis and A. Rufer, "A modular multiport power electronic transformer with integrated split battery energy storage for versatile ultra fast EV charging stations," *IEEE Trans. Ind. Electron.*, vol. 62, no. 5, pp. 3213–3222, May 2015, doi: 10.1109/TIE.2014.2367237.
- [3] G. Waltrich, M. A. M. Hendrix, and J. L. Duarte, "Three-phase bidirectional DC/DC converter with six inverter legs in parallel for EV applications," *IEEE Trans. Ind. Electron.*, vol. 63, no. 3, pp. 1372–1384, Mar. 2016, doi: 10.1109/TIE.2015.2494001.
- [4] K.-Y. Lo, Y.-M. Chen, and Y.-R. Chang, "MPPT battery charger for stand alone wind power system," *IEEE Trans. Power Electron.*, vol. 26, no. 6, pp. 1631–1638, Jun. 2011, doi: 10.1109/TPEL.2010.2088405.
- [5] D.-G. Woo, D.-M. Joo, and B.-K. Lee, "On the feasibility of integrated battery charger utilizing traction motor and inverter in plug-in hybrid electric vehicles," *IEEE Trans. Power Electron.*, vol. 30, no. 12, pp. 7270–7281, Dec. 2015, doi: 10.1109/TPEL.2015.2396200.
- [6] D. Moon, J. Park,

- and S. Choi, "New interleaved current-fed resonant converter with significantly reduced high current side output filter for EV and HEV applications," *IEEE Trans. Power Electron.*, vol. 30, no. 8, pp. 4264–4271, Aug. 2015, doi: 10.1109/TPEL.2014.2360470.
- [7] X. Zhang, Z. Lu, X. Yuan, Y. Wang, and X. Shen, "L2-gain adaptive robust control for hybrid energy storage system in electric vehicles," *IEEE Trans. Power Electron.*, vol. 36, no. 6, pp. 7319–7332, Jun. 2021, doi: 10.1109/TPEL.2020.3041653.
- [8] Y. Shen, J. Xie, T. He, L. Yao, and Y. Xiao, "CEEMD-fuzzy control energy management of hybrid energy storage systems in electric vehicles," *IEEE Trans. Energy Convers.*, early access, Aug. 21, 2024, doi: 10.1109/TEC.2023.3306804.
- [9] Y. Takahashi, "Development of a personal mobility vehicle for short range transportation support," in *Proc. IEEE Int. Syst.*, vol. 8, Jun. 2016, pp. 295–297, doi: 10.1109/ISMS.2016.37.
- [10] S. Yun, W. Lee, J. Park, and K.-W. Gwak, "Development of a virtual environment-co-simulation platform for evaluating dynamic characteristics of self-balancing personal mobility," *IEEE Trans. Veh. Technol.*, vol. 70, no. 4, pp. 2969–2978, Apr. 2021, doi: 10.1109/TVT.2021.3061733.
- [11] S. Kim and F.-S. Kang, "Multifunctional onboard battery charger for plug-in electric vehicles," *IEEE Trans. Ind. Electron.*, vol. 62, no. 6, pp. 3460–3472, Jun. 2015, doi: 10.1109/TIE.2014.2376878.
- [12] T. Q. Pham, C. Nakagawa, A. Shintani, and T. Ito, "Evaluation of the effects of a personal mobility vehicle on multiple pedestrians using personal space," *IEEE Trans. Intell. Transp. Syst.*, vol. 16, no. 4, pp. 2028–2037, Aug. 2015, doi: 10.1109/TITS.2014.2388219. [13] Y. Won Chung, M. Young Chung, and D. Keun Sung, "Effect of personal mobility management in mobile communication networks," *IEEE Trans. Veh. Technol.*, vol. 52, no. 5, pp. 1254–1269, Sep. 2003, doi: 10.1109/TVT.2003.816639.
- [14] A. Kuperman, U. Levy, J. Goren, A. Zafransky, and A. Savernin, "Battery charger for electric vehicle traction battery switch station," *IEEE Trans. Ind. Electron.*, vol. 60, no. 12, pp. 5391–5399, Dec. 2013, doi: 10.1109/TIE.2012.2233695.
- [15] J. Min and M. Ordonez, "Bidirectional resonant CLLC charger for wide battery voltage range: Asymmetric parameters methodology," *IEEE Trans. Power Electron.*, vol. 36, no. 6, pp. 6662–6673, Jun. 2021, doi: 10.1109/TPEL.2020.3033982.
- [16] H. Karneddi and D. Ronanki, "Universal bridgeless nonisolated battery charger with wide-output voltage range," *IEEE Trans. Power Electron.*, vol. 38, no. 3, pp. 2816–2820, Mar. 2023, doi: 10.1109/TPEL.2022.3217943.
- [17] S.-K. Lim, H.-S. Lee, H.-R. Cha, and S.-J. Park, "Multi-level DC/DC converter for E-mobility charging stations," *IEEE Access*, vol. 8, pp. 48774–48783, 2020, doi: 10.1109/ACCESS.2020.2977663.
- [18] F. Musavi, M. Craciun, D. S. Gautam, and W. Eberle, "Control strategies for wide output voltage range LLC resonant DC–DC converters in battery chargers," *IEEE Trans. Veh. Technol.*, vol. 63, no. 3, pp. 1117–1125, Mar. 2014, doi: 10.1109/TVT.2013.2283158.
- [19] Y. Bak, "Hardware-simulator development and implementation of battery charger for personal mobility devices," *J. Power Electron.*, vol. 23, pp. 211–218, Feb. 2023, doi: 10.1007/s43236-022-00580-1.
- [20] M.-G. Jeong, S.-H. Kim, and C. Yoo, "Switching battery charger integrated circuit for mobile devices in a 130-nm BCD MOS process," *IEEE Trans. Power Electron.*, vol. 31, no. 11, pp. 7943–7952, Nov. 2016, doi: 10.1109/TPEL.2016.2514518.
- [21] N. Shafiei, M. Ordonez, M. Craciun, C. Botting, and M. Edington, "Burst mode elimination in high-power LLC resonant battery charger for electric vehicles," *IEEE Trans. Power Electron.*, vol. 31, no. 2, pp. 1173–1188, Feb. 2016, doi: 10.1109/TPEL.2015.2420573.
- [22] R. Metidji, B. Metidji, and B. Mendil, "Design and implementation of a unity power factor fuzzy battery charger using an ultrasparse matrix rectifier," *IEEE Trans. Power Electron.*, vol. 28, no. 5, pp. 2269–2276, May 2013, doi: 10.1109/TPEL.2012.2211107.
- [23] B.-Y. Chen and Y.-S. Lai, "New digital-controlled technique for battery charger with constant current and voltage control without current feedback," *IEEE Trans. Ind. Electron.*, vol. 59, no. 3, pp. 1545–1553, Mar. 2012, doi: 10.1109/TIE.2011.2167115.

[24] Y.-H. Jung, J.-H. Jung, H.-E. Jeong, J.-H. Jung, J.-S. An, H.-A. Ahn, S.-K. Hong, and O.-K. Kwon, "A fast and highly accurate battery charger with accurate built-in resistance detection," *IEEE Trans. Power Electron.*, vol. 33, no. 12, pp. 10051–10054, Dec. 2018, doi: 10.1109/TPEL.2018.2830747.

[25] Z. Huang, G. Wang, J. Yu, and X. Qu, "A novel clamp coil assisted IPT battery charger with inherent CC-to-CV transition capability," *IEEE Trans. Power Electron.*, vol. 36, no. 8, pp. 8607–8611, Aug. 2021.

[26] P.-J. Liu and L.-H. Chien, "A high-efficiency integrated multimode battery charger with an adaptive supply voltage control scheme," *IEEE Trans. Power Electron.*, vol. 33, no. 8, pp. 6869–6876, Aug. 2018, doi: 10.1109/TPEL.2017.2761816.

[27] L. Zhang, Q. Yin, W. Zhu, L. Lyu, L. Jiang, L. H. Koh, and G. Cai, "Research on the orderly charging and discharging mechanism of electric vehicles considering travel characteristics and carbon quota," *IEEE Trans. Transp. Electrification*, early access, Jul. 19, 2023, doi: 10.1109/TTE.2023.3296964.

[28] Y. Bak, Y. J. Lee, and K.-B. Lee, "Dynamic characteristic improvement of phase-shift full-bridge center-tapped converters using a model predictive control," *IEEE Trans. Ind. Electron.*, vol. 69, no. 2, pp. 1488–1497, Feb. 2022, doi: 10.1109/TIE.2021.3057038.

[29] E. Fuentes, C. A. Silva, and R. M. Kennel, "MPC implementation of a quasi-time-optimal speed control for a PMSM drive, with innermodulated FS-MPC torque control," *IEEE Trans. Ind. Electron.*, vol. 63, no. 6, pp. 3897–3905, Jun. 2016, doi: 10.1109/TIE.2016.2519326.

[30] C. Wang, M. Yang, W. Zheng, J. Long, and D. Xu, "Vibration suppression with shaft torque limitation using explicit MPC-PI switching control in elastic drive systems," *IEEE Trans. Ind. Electron.*, vol. 62, no. 11, pp. 6855–6867, Nov. 2015, doi: 10.1109/TIE.2015.2438055.